Since January 2020 Elsevier has created a COVID-19 resource centre with free information in English and Mandarin on the novel coronavirus COVID-19. The COVID-19 resource centre is hosted on Elsevier Connect, the company's public news and information website.

Biomedical Signal Processing and Control 68 (2021) 102812

Contents lists available at ScienceDirect

Biomedical Signal Processing and Control

journal homepage: www.elsevier.com/locate/bspc

A novel DeepNet model for the efficient detection of COVID-19 for symptomatic patients

Alavikunhu Panthakkan [a,*], S.M. Anzar [b,*], Saeed Al Mansoori [c], Hussain Al Ahmad [a]

[a] College of Engineering and IT, University of Dubai, United Arab Emirates
[b] TKM College of Engineering, Kollam, India
[c] Applications Development and Analysis Section, Mohammed Bin Rashid Space Centre (MBRSC), United Arab Emirates

ARTICLE INFO

Keywords:
COVID-19
Lung X-rays
Clinical diagnosis
Artificial intelligence
Deep learning
COVID-DeepNet

ABSTRACT

The novel Coronavirus (COVID-19) disease has disrupted human life worldwide and put the entire planet on standby. A resurgence of coronavirus infections has been confirmed in most countries, resulting in a second wave of the deadly virus. The infectious virus has symptoms ranging from an itchy throat to Pneumonia, resulting in the loss of thousands of human lives while globally infecting millions. Detecting the presence of COVID-19 as early as possible is critical, as it helps prevent further spread of disease and helps isolate and provide treatment to the infected patients. Recent radiological imaging findings confirm that lung X-ray and CT scans provide an excellent indication of the progression of COVID-19 infection in acute symptomatic carriers. This investigation aims to rapidly detect COVID-19 progression and non-COVID Pneumonia from lung X-ray images of heavily symptomatic patients. A novel and highly efficient COVID-DeepNet model is presented for the accurate and rapid prediction of COVID-19 infection using state-of-the-art Artificial Intelligence techniques. The proposed model provides a multi-class classification of lung X-ray images into COVID-19, non-COVID Pneumonia, and normal (healthy). The proposed systems' performance is assessed based on the evaluation metrics such as accuracy, sensitivity, precision, and f1 score. The current research employed a dataset size of 7500 X-ray samples. The high recognition accuracy of 99.67% was observed for the proposed COVID-DeepNet model, and it complies with the most recent state-of-the-art. The proposed COVID-DeepNet model is highly efficient and accurate, and it can assist radiologists and doctors in the early clinical diagnosis of COVID-19 infection for symptomatic patients.

1. Introduction

The COVID-19 pandemic, caused by the micro-organism 'SARS-CoV-2', has profoundly impacted every nation's social and economic structures and disrupted all humans' daily lives [1–5]. A single-stranded RNA virus (COVID-19) is currently the leading cause of death in the vast majority of countries across the globe [6]. The second wave of the deadly disease has wrought havoc on many major cities (Texas, California, Belgium, Delhi, Mumbai, etc.) worldwide. Hospitals and crematoriums are at capacity, so funerals are being held in parking lots. However, the pandemic has now engulfed many smaller cities, towns, and villages, with the resulting devastation largely unreported. Fig. 1 shows the updated and region-by-region data on confirmed cases of COVID-19 reported by WHO [7]. Scientists, engineers, doctors, and policymakers have widely researched the implications, and consequences of COVID-19 infection and the subsequent preventive measures [8–11]. Numerous efforts are exercised in various domains to obtain the best treatment practices and investigate the short-term and long-term consequences of the COVID-19 infection on human beings and the environment [4,10].

This deadly disease is difficult to diagnose and treat due to its rapid spread and mutation effects, further complicating matters. Reports reveal that approximately 80% of patients recover without significant complications from the disease, and COVID-19 can spread through silent carriers. They express little or no symptoms of the disease. However, one out of every six infected individuals is reported to suffer from critical illness and breathing ailments [12,13]. In severe cases, the infection has led to severe Pneumonia and other complications required to be treated at well-equipped treatment facilities. In terms of symptoms, age profile, and geographic spread, the second wave of the Covid-19 pandemic has a few minor but distinguishing characteristics. Various methods such as Swab test, Nasal aspirate, Tracheal aspiration, Sputum test, and Blood

* Corresponding author.
E-mail addresses: apanthakkan@ud.ac.ae (A. Panthakkan), anzarsm@tkmce.ac.in (S.M. Anzar).

https://doi.org/10.1016/j.bspc.2021.102812
Received 13 February 2021; Received in revised form 5 May 2021; Accepted 23 May 2021
Available online 27 May 2021

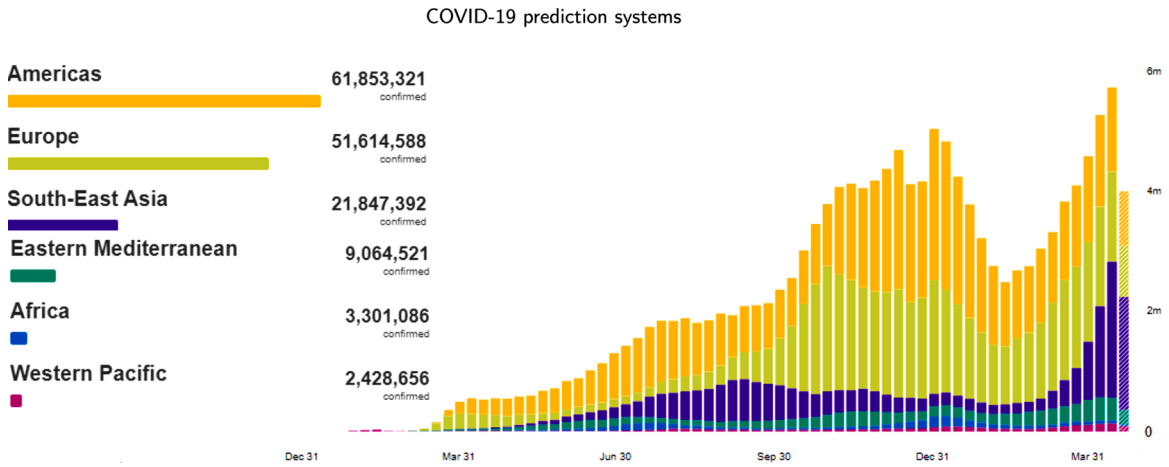

Fig. 1. COVID-19 confirmed cases globally (from December 2019 to March 2021) [7].

test are used to detect the coronavirus's presence [1,2,12]. General laboratory findings revealed decreased lymphocyte count and increased C-reactive protein (CRP) level in test samples. At present, polymerize chain reaction (PCR), and antibody testing are widely used for testing COVID-19 suspects by various healthcare facilities across the globe. The PCR test is particular but has a lower sensitivity of 65–95%, indicating that the test gives false-negative results [14]. Another issue related to the PCR test is the time it takes, usually more than 24 h. Moreover, antibody tests can also result in false-positive results [14].

Detection of the COVID-19 infection is vital as it allows governments and health care facilities to adopt appropriate measures to isolate the infected person, thereby preventing further spread of the disease and assists in the diagnosis, treatment, and management of the patients effectively [1,2,15]. A variety of studies have reported COVID-19 detection from a smaller set of original X-ray images. However, its impact on an extensive database has not been thoroughly investigated. This paper proposes a novel, highly accurate, and efficient AI deep learning model for the rapid and non-invasive detection of COVID-19 for acutely symptomatic patients whose pathology infection can be screened using X-ray images. A total of 7500 X-ray samples were used in the current study. COVID-19 detection through X-ray imaging is cost-effective and poses minimal radiation risks to human health compared to CT imaging [16,17]. Thus the reported method can be used as an alternative solution for detecting COVID-19.

The rapid growth of COVID-19 has increased the need for the development of automated AI-based detection systems for managing the pandemic and its implications [3,18,19]. Recent studies reveal that Deep Neural Networks enhance the efficiency of imaging-based classifications in various medical diagnoses [18,20–22]. It has been successfully employed in many clinical applications such as brain disease classification, breast cancer identification, diabetic retinopathy, skin cancer classification, lung segmentation, fundus image segmentation, identification of Arrhythmias, and Pneumonia [18,20,23,24]. Deep learning (DL) is a subset of machine learning algorithms that focus on direct learning from various data representations. It denotes the machine learning methods that use complex computational layers, stacked one after the other [25]. DL systems allow the designing of an end-to-end model to attain superior performance without the need for the feature extraction procedure [11,25].

The presented method proposes a highly accurate and efficient deep learning model that can be used for the faster screening of COVID-19. The proposed COVID-DeepNet model was trained with 6000 lung X-ray images, and it classifies lung X-ray images into COVID-19, non-COVID Pneumonia, and normal. For each category, 2500 lung X-ray image samples were considered. About 80% of the X-ray images were used for training and validation, and the remaining 20% images were used for testing purposes. The methods proposed in this study are highly efficient and accurate when compared to previously used approaches. The proposed COVID-DeepNet model provided a classification accuracy of 99.67%. Accuracy, sensitivity, precision, and f1 score evaluations of the proposed deep learning model demonstrated that the method could be implemented effectively for the rapid diagnosis of COVID-19 and non-COVID Pneumonia. The presented technique could be applied in combination with the antibody test for the faster screening of COVID-19. Consequently, by employing the proposed method, we could overcome the delay involved in the PCR testing. Hence, it can serve as an alternative solution for the rapid detection of COVID-19 for acutely symptomatic patients. Additionally, the AI solutions presented here would be beneficial for radiologists if the COVID-19 test kits are not available or inefficient, or if false negatives are critical, or if the expense in testing is not viable, or if extended time is a requirement for procuring the test results.

1.1. Organization of the paper

The remainder of the paper is organized as follows. The following section provides a brief overview of the relevant works with COVID-19 detection from lung X-rays. Section 3 provides the motivation behind and the implementation details of the proposed COVID-DeepNet model. The results of the experiments are detailed in Section 4 along with the database and experimental setup. The paper ends with a conclusion in Section 5.

2. Related work

Recent research in radio diagnostics has shown that the inflammation of the alveoli can be identified using an X-ray scan of the lungs [20]. Analysis by Chan et al. depicted deviations in pulmonary X-ray images even before the onset of COVID-19 symptoms [27]. This study indicated the significance of lung radiography in the early diagnosis of COVID-19 with adequate sensitivity in detecting GGO (ground-glass opacity), the first sign of COVID-19 [1,2,4,12–14,18,28,29]. The GGO on a lung X-ray is so perceived due to the-frosted-glass-on-a-shower-door-like appearance. The presence of GGO means that some portion of the lungs appear as a hazy shade of grey (as alveoli start filling with fluid instead of air), but not hazy enough to obscure the underlying pulmonary vessels or bronchial walls [14,28–30]. In severe cases of infections, instead of a 'ground-glass' appearance, solid white consolidations tend to be observed. Consolidations in the lungs occur when air spaces are filled with fluid. More fluid accumulation in the alveoli and the hazy lung opacity increases and becomes dense enough to obscure the underlying pulmonary vessels or bronchial walls [28].

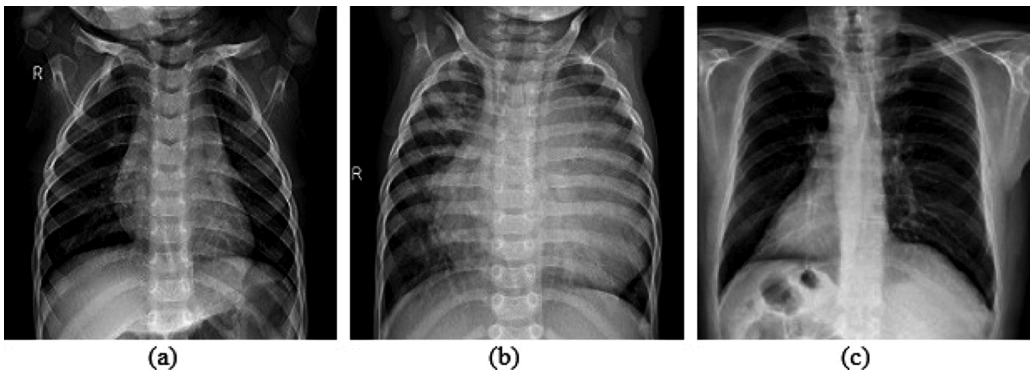

Fig. 2. X-ray Images: (a) Normal (b) non-COVID Pneumonia (c) COVID-19.

Table 1
Non-COVID Pneumonia and COVID-19 features present in lung X-ray/CT images [11,26].

Features	Non-COVID Pneumonia	COVID-19
Ground Glass Opacity's (GGO)	Present unilaterally involving mostly the central zone of the lung	Present bilaterally involving mostly the peripheral zone of the lung
Solid white consolidation	Mainly involves central zone of the lung and is unilateral	Mainly involves peripheral and lower zone of the lung and are bilaterally symmetric during the starting stage
Crazy paving pattern	White line against GGO is not observed	White line against GGO is observed
In Lung Imaging	Pleural effusion, large lymph nodes pericardial fluid collection and lung cavities are observed	Pleural effusion, large lymph nodes pericardial fluid collection, subpleural spacing, and lung cavities not mostly observed

Consolidation in the lungs is observed in the peripheral, lower, and bilaterally symmetric lung regions during the starting stage. Gradually the swelling of the interstitial space along the walls of the lung lobule makes the walls thicker and results in a crazy-paving pattern (white lines against the GGO) to appear in the lung CT. Pleural and pericardial effusion (fluid collection), lymphadenopathies (large lymph nodes), subpleural spacing, and lung cavities are not observed in most COVID-19 lung radiographs [1,2,4,10,11,28,29,31]. Fig. 2 shows a comparison of the X-ray image of a healthy person with those infected with non-COVID Pneumonia and COVID-19. Table 1 illustrates the common non-COVID Pneumonia and COVID-19 features observed in lung X-ray/CT images [11,26]. According to recent research findings, combining clinical X-ray analysis with laboratory results may help in the faster and efficient diagnosis of COVID-19 [1,2,4,11,29].

A plethora of studies has been performed to investigate automated lung X-ray imaging to distinguish patients with Pneumonia and COVID-19 using the deep learning method. Research by Ozturk et al. [11] presented a model that detects COVID-19 infection from raw lung X-ray imagery. This model was developed for both binary and multi-class settings. For the multi-class case with COVID-19, Pneumonia, and normal, an accuracy of 87.02% was reported. In [20], the authors made a comparative analysis on the use of MobileNet v2, Resnet50, Inception v3, Inception-ResNet-v2, DenseNet201, VGG16, and VGG19 for the three-class classification of COVID-19, Pneumonia, and normal cases from the X-ray images. Their Inception-ResNet-v2 and Densnet201 models provided a classification accuracy of 92.18% and 88.09%, respectively. Wang et al. reported a COVID-Net model for the classification of X-ray images of COVID-19(+), COVID-19(-), Pneumonia, and normal (healthy) individuals [32]. This research considered 358-COVID-19, 5526-non COVID Pneumonia, and 8066-normal X-ray images for performing three-class classification and reported an accuracy of 93.33% for their proposed model.

For the two and three class classification cases, Rubina et al. [33] proposed CNNs models. They created a new CNN model for detecting COVID-19 automatically with a reported accuracy of 93.75%. In [34], the authors proposed a Densenet-121 model for detecting COVID-19. They employed a transfer learning technique using CheXNet model trained on a dataset of 420 images. The authors employed two-class and three-class classifications to evaluate the model's robustness, achieving 96.49% and 93.71% accuracy, respectively. In [35], the authors proposed an E-DiCoNet for classifying the chest X-ray images into COVID-19, normal, and Pneumonia. They achieved an accuracy of 94.07% with their model for a sample size of 900 each. Makris et al. used nine well-known CNNs to classify X-Ray images into COVID-19, Pneumonia, and normal [36]. Their findings suggested that CNN's can detect respiratory diseases with high accuracy, though many image samples are required for training the network. They reported an overall accuracy of 95% for their VGG16 and VGG19 models. Siddhartha et al. proposed a COVIDLite model for the screening of COVID-19 X-ray images [37]. They claimed that their proposed model is light and ideal for web applications.

Ioannis D. Apostolopoulos et al. reported a three-class classification of COVID-19, Pneumonia, and normal lung X-ray images using transfer learning of Deep CNN [19]. They claimed a testing accuracy of 93.48% with the VGG-19 model. This study was performed on 224 COVID-19, 700 Pneumonia, and 500 normal X-ray image samples. Sohaib Asif et al. [38] proposed a method based on deep convolutional neural networks (DCNN) for detecting COVID-19. This study's dataset comprised 864-COVID-19, 1345- viral Pneumonia, and 1341-normal lung X-ray images. The experimental results indicated that the model achieved an accuracy of 98%. In [39], the authors proposed a COVIDScreen model for the differential diagnosis of COVID-19 using lung X-rays. The reported model achieved a prediction accuracy of 98.67% on standard datasets. [40] proposed an Xception model using a transfer learning approach for the automated diagnosis of COVID-19 and reported an accuracy of 99.12%. COVID-19 detection using deep learning models such as MobileNetv2 and Squeeze Net was presented in studies conducted by Toğaçar et al. [41]. The suggested method provided a prediction accuracy of 99.27% for the database of 295-COVID-19, 98-Pneumonia, and 65-normal X-ray images.

Previous research reveals that deep learning methods can improve computer vision tasks like image recognition. With the state-of-the-art artificial intelligence techniques, most approaches recorded a prediction accuracy of 90–100% [6]. Furthermore, most of the published methods employed X-ray images of limited size, which is not advisable for deep learning tasks. Consequently, the efficiency of the reported techniques tested on a small dataset cannot be generalized on a considerably large dataset. As a result, the current research employed a more extensive dataset (7500 Lung X-ray samples), despite the practical

difficulties. The proposed method serves as an alternative solution for detecting COVID-19 for patients with lung infections that can be screened using X-ray images.

3. Methods

Deep learning techniques are popular applications employed mainly due to data flooding and growing computing power (GPUs) [25]. Deep learning-based algorithms differ in various aspects, viz. pre-processing steps, network architectures, model hyper-parameters, methods to configure and optimize CNN parameters, and strategies to handle skewed distribution of data [42]. Deep learning algorithms require several epochs of training and validation to achieve optimal performance [43]. This paper demonstrates the efficacy of a novel, highly accurate, and proficient COVID-DeepNet model for detecting COVID-19 and non-COVID Pneumonia for acutely symptomatic patients. The proposed deep learning model distinguishes an X-ray image into COVID-19, non-COVID Pneumonia, and normal at an efficient rate.

3.1. Foundation of the proposed model

Convolutional Neural Networks (CNNs) are the most popular deep learning algorithms with highly successful Artificial Neural Networks (ANNs) [42]. CNN's are widely used in computer vision image analysis and pattern recognition (image classification) applications [3,21,22,32,38,43,42,44]. The 7-layer CNN LeNet-5 is the foundation of modern CNN architecture. These techniques have proved to be efficient in the clinical diagnosis of various diseases [45]. All versions of CNN are the variants of LeNet-5 architecture. The internal architecture of LeNet-5 architecture [42] is briefly discussed as follows:

- Layer1: Convolutional layer with six feature maps or filters of size 5 × 5 and a stride of 1. In layer1, the image dimension is reduced from 32 × 32 × 1 to 28 × 28 × 6.
- Layer2: Average pooling layer with a filter size 2 × 2 and a stride of 2. In Layer2, the image dimension is reduced to 14 × 14 × 6.
- Layer3: Convolutional layer with 16 feature maps of size 5 × 5 and a stride of 1. Only 10 out of 16 feature maps are connected to the 6 feature maps of the previous layer.
- Layer4: Average pooling layer with filter size 2 × 2 and a stride of 2. Layer4 has 16 feature maps, and the output is reduced to 5 × 5 ×16.
- Layer5: Fully connected convolutional layer with 120 feature maps each of size 1 × 1. Each unit in layer5 is connected to all the 400 nodes (5 × 5 ×16) in the layer4.
- Layer6: Fully connected layer with 84 units.
- Layer7: Fully connected softmax output layer with 10 possible values corresponding to the digits from 0 to 9.

3.1.1. Convolution layer

The proposed AI deep learning architecture consisted of several convolution layers for extracting features from the input by applying convolution kernels (filters). The initial convolution layers of CNN detect the general components such as the edges of an image. More abstract features, such as image-specific features, were taken out by the latter layers [42]. The output feature value at location (i, j) with kth feature map in lth layer is, given by,

$$z^{l}_{i,j,k} = w^{l^T}_{k} x^{l}_{i,j} + b^{l}_{k} \tag{1}$$

where w^{l}_{k} is the weight vector and b^{l}_{k} are bias values of kth filter in lth layer. In general, convolution function is defined as,

$$z^{l} = h^{l-1} * w^{l} \tag{2}$$

Where z^{l}: pre-activation output layer l, h^{l}: activation of layer l, W: (weights) learnable parameter.

3.1.2. Activation functions

The convoluted output was then passed via an activation function. Activation functions are small, non-linear modifications that can be applied to each neuron's output before passing on the convoluted value. Typical activation functions are sigmoid, tanh, ReLU (Rectified Linear Unit), Leaku ReLU, ELU (Exponential Linear Unit), and softmax [42,43]. The same activation function was applied to every neuron in a given layer. The activation function f when applied to the convolved feature $z^{l}_{i,j,k}$ gives

$$a^{l}_{i,j,k} = f(z^{l}_{i,j,k}) \tag{3}$$

Sigmoid activation function is defined as [42]

$$\sigma(z_i) = \frac{1}{\sum_{j=1}^{k} e^{z_j}} \tag{4}$$

The tanh activation function on z is defined as [42]

$$f(z) = A \tanh(Sz) \tag{5}$$

where A is amplitude and S is slope of the function.

ReLU activation function is defined as [43]

$$\mathrm{ReLU}(z_i) = \max(0, z_i) \tag{6}$$

Softmax activation function is defined as [43]

$$\mathrm{softmax}(z_i) = \frac{e^{z_i}}{\sum_{j=1}^{k} e^{z_j}} \tag{7}$$

3.1.3. Pooling layer

Each convolution layer was followed by a sub-sampling layer to down-sample the dimension of the feature maps by 2 [43]. Sub-sampling layers were 2 × 2 pooling layers. The used pooling methods were average pooling and max pooling [42]; a pooling later enabled adjustment of the size of the data that flows through the network [25]. This technique is often used to reduce the size of an image to speed up the processing. The average pooling function is defined as [42],

$$h^{l}_{x,y} = \frac{1}{hw} \sum_{i,j=1}^{h,w} h^{l-1}_{x+i,y+j} \tag{8}$$

The max pooling function is defined as [42],

$$h^{l}_{x,y} = \sum_{i,j=1}^{h,w} h^{l-1}_{x+i,y+j} \tag{9}$$

3.1.4. Fully connected layer

In a fully connected (FC) layer, a group of neurons receives input from each preceding neuronal layer. They are also known as a dense layer or FC and are designed with different deep learning methods. Nets such as multi-layer perceptrons (MLPs) or fully connected nets contain a stack of dense layers [25,42].

3.1.5. Loss function

Loss functions help to optimize CNN's parameters. The loss function here represents the difference between the actual output value and the CNN's predicted value. This value is required to train weights and network bias. Cross entropy is a measure of matching the distribution of predictions and the actual distribution. When considering multiple output labels, categorical cross-entropy defined as follows were used, and each input was assigned to just one label [42].

$$J = -\frac{1}{N}\sum_{i=1}^{n}\sum_{j=1}^{M} z_{ij}\log(\widehat{z}_{ij}) \tag{10}$$

Where N is the number of elements for the training set, and M is the number of categories (class), z is target output and $\widehat{z}$ is the output of CNN.

3.1.6. Optimization algorithms

Optimization of algorithms allows the neural networks to train faster. Error (loss) J is a function of the model's internal parameters, i.e., weights and bias. The back-propagation reduces the prediction error in a neural network. The network's weights and bias are adjusted to minimize error during back-propagation of errors to a previous stage. The gradient descent approach was used along with the differentiable loss function [42,46]. Updated weight and bias is given by,

$$w(k+1) = w(k) - \eta * \mathrm{dw} \tag{11}$$

$$b(k+1) = b(k) - \eta * \mathrm{db} \tag{12}$$

$$\mathrm{dw} = \frac{\mathrm{dJ}}{\mathrm{dw}} \tag{13}$$

$$\mathrm{db} = \frac{\mathrm{dJ}}{\mathrm{db}} \tag{14}$$

where η is learning rate.

3.1.7. Regularization

Many neural networks have an issue with over-fitting. As soon as a network begins memorizing the training data and is over-fitting, the training was stopped. Regularization strategies were used to extend the onset of over-fitting. Methods of regularization allowed us to train networks for a longer duration before they were over-fitted, thus providing better efficiency. One such method is called the 'dropout' to delay over-fitting and is used with the inclusion of a dropout layer in deep networks [25]. The dropout layer made no computation but disconnected some of the neurons in the previous layer for a temporary period. These disconnected neurons were isolated and showed no involvement in any calculations or updates. The neurons restored their connections, and once the epoch was complete and all the weights were modified. The intention behind the dropout was to prevent any of the neurons from being over-specialized. In short, the dropout helped to diminish over-fitting by spreading out learning across all the neurons [43]. The regularization types L1 and L2 operated by introducing related terms in the loss function and modifying the weight update rule. These regularizations were termed as L1 and L2 norm of weight matrices [43].

$$\mathrm{Cost\ \ function} = \mathrm{Loss} + \mathrm{Regularization\ \ term} \tag{15}$$

L1 regularization:

$$\mathrm{Cost\ \ function} = \mathrm{Loss} + \lambda\sum|w| \tag{16}$$

$|w|$ is absolute value of weights. λ is regularization hyper parameter.

L2 regularization:

$$\mathrm{Cost\ \ function} = \mathrm{Loss} + \lambda\sum||w||^2 \tag{17}$$

$$\text{where, } ||w||^2 = \sum_i\sum_j w_{ij}^2 \tag{18}$$

An alternative approach of regularization is called 'batch normalization'. This method was applied to adjust the numerical values that developed out of a computational layer. The rationale behind batch normalization is to normalize the results after a layer of computation is formed but before it is passed to the activation unit. The layer that performed batch normalization gathered all the values flowing out of a computational layer over the transit of a batch [25].

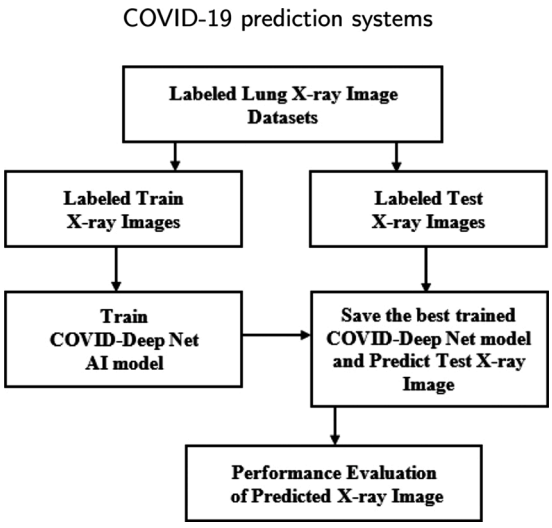

Fig. 3. Block diagram of the proposed AI deep learning method.

$$\mathrm{BN}(z_i) = \gamma_i\widehat{z_i} + \beta_i \tag{19}$$

$$\widehat{z_i} = \frac{z_i - E[z_i]}{\sqrt{\mathrm{Var}[z_i]}} \tag{20}$$

Here, γ, and β are learnable parameters.

3.2. Pseudo code of the proposed model

The block diagram of the proposed methods is depicted in Fig. 3 and the pseudo code of the proposed model is detailed below.

- begin
  - –The labelled X-ray image data set was split into train and test;
  - –Deep learning model (COVID-DeepNet) was selected;
  - –The size of the first layer of the AI model was set to 64 × 64 and the last layer to 3;
  - –The AI model was trained using the training data set and save the best-trained model;
  - –Prediction of the X-ray image (test data set) type using the best-trained model was performed;
  - –The predicted results with the ground truth values were compared;
  - –The model performance was evaluated and noted;
- end

3.3. Proposed COVID-DeepNet model

In this paper, a highly accurate and efficient COVID-DeepNet model is proposed to classify X-ray images into COVID-19, non-COVID Pneumonia, and normal. The block diagram of the proposed COVID-DeepNet model is depicted in Fig. 4, and detailed architecture about various hidden layers is described in Table 2. The model was built from scratch, training the network rigorously to perform accurate predictions of the diseases. The COVID-DeepNet performs conventional feature extraction and classification within a unified framework. In the current research, the number of hidden layers for the proposed architecture has been customized. The proposed COVID-DeepNet architecture is a straightforward and highly efficient method in predicting diseases with an exceptional testing accuracy of 99.67%. In the proposed COVID-DeepNet model, the input image size is resized to 64 × 64 in the first layer, and at the output, the number of classification types is set to three. During the training stage, 50% drop out is implemented in the dense,

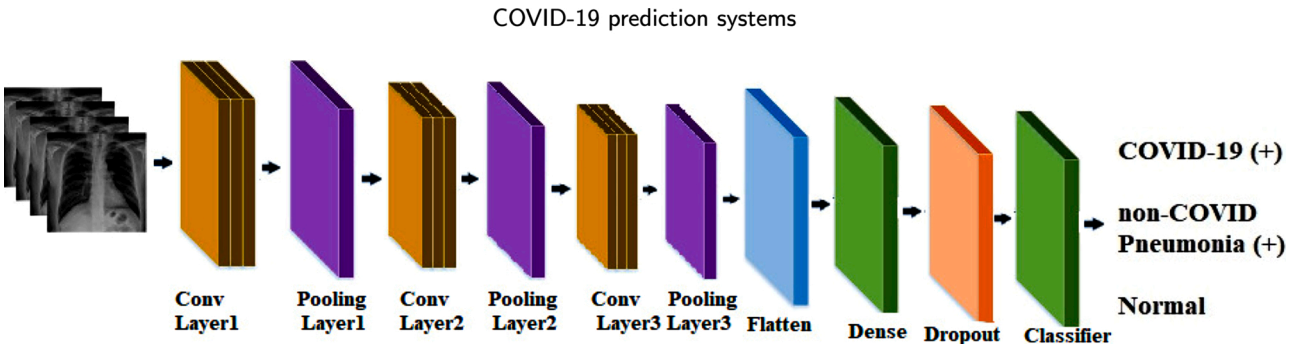

Fig. 4. Proposed COVID-DeepNet model for COVID-19 detection.

Table 2
Proposed COVID-DeepNet model.

Layer (type)	Output shape	Parameters
Conv2d (Conv2D)	(None, 62, 62, 32)	896
Max pooling2d (MaxPooling2D)	(None, 31, 31, 32)	0
Conv2d (Conv2D)	(None, 29, 29, 64)	18,496
Max pooling2d (MaxPooling2D)	(None, 14, 14, 64)	0
conv2d (Conv2D)	(None, 12, 12, 128)	73,856
Max pooling2d (MaxPooling2D)	(None, 6, 6, 128)	0
Flatten (Flatten)	(None, 4608)	0
Dense (Dense)	(None, 512)	2,359,808
dropout (Dropout)	(None, 512)	0
Dense (Dense)	(None, 3)	1539
Total params: 2,454,595		
Trainable params: 2,454,595		
Non-trainable params: 0		

fully connected layers to avoid overfitting. ReLU and softmax activation functions were used in the hidden and output layers, respectively.

4. Results and discussion

4.1. Database and experimental set-up

The proposed work (COVID-DeepNet model) is based on a multi-class classification approach for the rapid diagnosis of COVID-19 and non-COVID Pneumonia. Python version 3.6.9 was used to build the model. This research was carried out using open-source software libraries such as Tensor-Flow and Keras, which were built on top of Tensor-Flow. Google Colab was used as the development environment.

Lung X-ray images, which are updated continuously from various open sources, were employed for the experimentation. The X-ray images were considered from the Kaggle, Cohen [47], and Wang et al. [48] data sets. The images were labelled by the radiologist as COVID-19 (2500), non-COVID Pneumonia (2500), and normal (2500). Twenty percent of the COVID 19 X-ray images (500) were augmented using translation, flipping, and rotation operations, resulting in a total of 2500 images. To prevent network bias, we employed the exact dataset sizes for all three classes. The sample X-ray images are shown in Fig. 2. Out of the total 7500 lung X-ray images considered for the study, 80% (6000) samples were used for training, and 20% (1500) were used for testing the proposed AI deep learning model. The labelled X-ray images were pre-processed, and all the X-ray images with varied sizes were scaled to a uniform size of 64 × 64 before the training process.

The training process in this research included both training and validation stages. Hence, the total training samples were further divided into two – 90% for model training (5400) and 10% for internal validation (600). A validation test was performed along with the training process to check the correctness of the training during the model development stage. The training of the proposed COVID-DeepNet model was performed batch-wise with a size of 50. The networks were trained for 100 epochs. The performance of the proposed multi-class classification models was evaluated based on accuracy, sensitivity, specificity, precision, and f1 score [25,45].

4.2. Performance of the proposed model

Batches containing 50 samples and 100 epochs for training the network were considered in the current research. The reported training and validation accuracy were estimated to be 94.97% and 95.65%, at

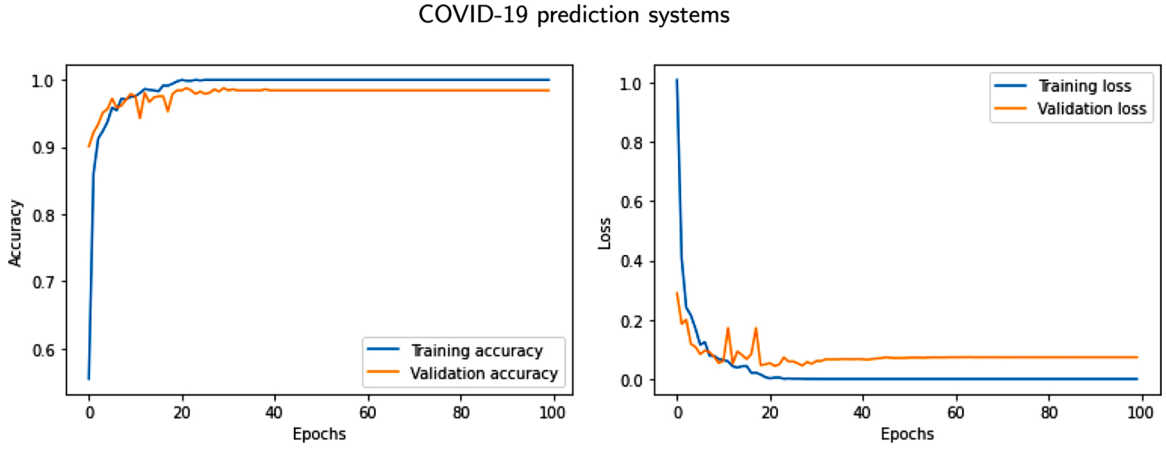

(a) Accuracy verses epochs (b) Loss verses epochs

Fig. 5. Training accuracy/loss versus epochs for the proposed COVID-DeepNet.

Table 3
Accuracy & loss versus epochs for training & validation.

Epochs	Accuracy		Loss	
	Training	Validation	Training	Validation
5	0.9497	0.9565	0.1323	0.1079
10	0.9769	0.9791	0.0597	0.0533
15	0.9847	0.9739	0.0460	0.0807
20	0.9982	0.9843	0.0058	0.0491
25	0.9986	0.9876	0.0026	0.0589
50	1.0000	0.9897	3.8643×10^{-6}	0.0707
75	1.0000	0.9913	1.3810×10^{-6}	0.0700
100	1.0000	0.9955	2.6805×10^{-6}	0.0632

the fifth epoch training, whereas the training and validation loss obtained are 0.1323 and 0.1079, respectively. Accuracies and loss during training and validation in the 50th epoch are (1.0000 and 0.9897) and (3.8643×10^{-6} and 0.0707), respectively. During the 100th epoch, the training and validation accuracy were found to be 100% and 99.55%, whereas the training and validation loss obtained are 2.6805×10^{-6} and 0.0632, respectively. In our proposed model, both the training and validation performance are comparable. The training and validation accuracy improves up to 50 epochs and remains unchanged after that. Since the training and validation accuracies are in the same range, there is no over fitting. This is evident from Fig. 5 (a and b), and Table 3 [training accuracy and loss versus epoch]. An advantage of the proposed design is that the network saves the best-trained model out of the 100 training epochs.

The proposed COVID-DeepNet model was also tested using 20% of

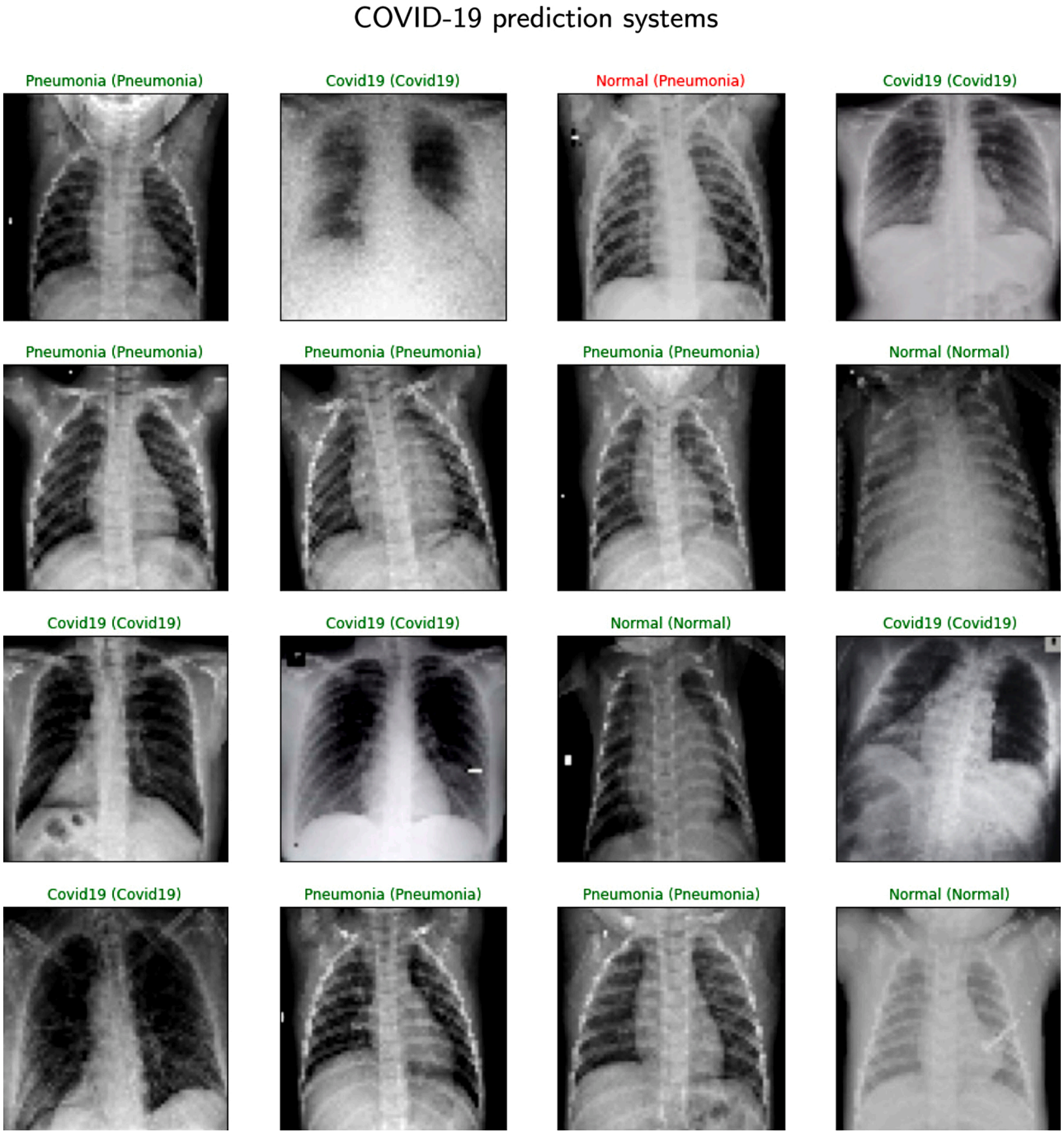

Fig. 6. X-ray image detection with the proposed COVID-DeepNet model.

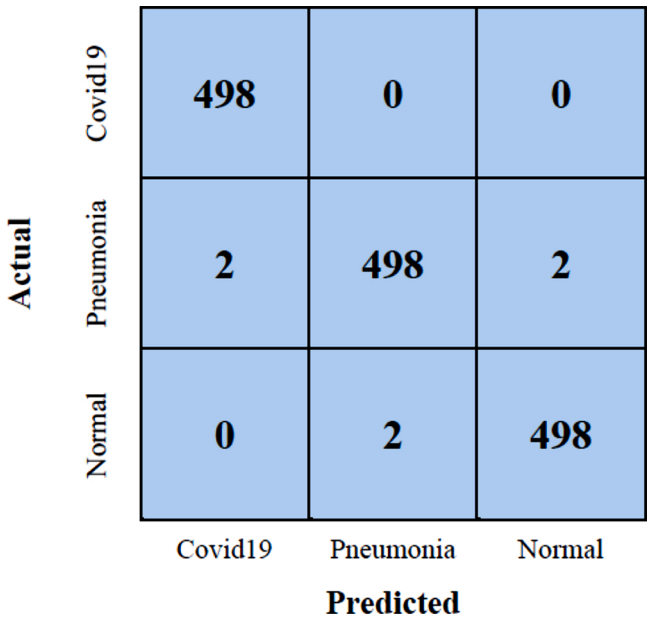

Fig. 7. Confusion matrix with the proposed models.

Table 4
Performance of the proposed COVID-DeepNet model.

Health condition	Accuracy	Sensitivity	Precision	f1 score
COVID-19	0.9966	0.9965	0.9966	0.9965
Non-COVID Pneumonia	0.9967	0.9964	0.9965	0.9966
Normal	0.9968	0.9966	0.9967	0.9967
Average	0.9967	0.9965	0.9966	0.9966

the total X-ray input samples. The predicted samples against the ground-truth images, and confusion matrix with the proposed model are presented in Fig. 6, and Fig. 7 respectively. The average accuracy (0.9967) [normalized], sensitivity (0.9965), precision (0.9966), and f1 score (0.9966) with the proposed COVID-DeepNet model are depicted in Table 4. The time elapsed for training the proposed COVID-DeepNet model in Google Colab Platform with GPU was 32 min, and for testing it took 1.5 seconds. These results reveal the efficacy of the proposed model for the multi-class classification of X-ray images into COVID-19, non-COVID Pneumonia, and normal.

4.3. Significance of the proposed model

Most studies in literature treated COVID-19 detection either as a two-class classification [11,49] or as a three-class classification task [11,20,19,32,38,41,50]. The reported method is a three-class classification approach for the detection of COVID-19, non-COVID Pneumonia, and Normal. The current research compared the performance of the proposed COVID-DeepNet model with the relevant and related COVID-19 detection techniques that used lung X-rays as their image types. Its performance is compared with the state-of-the-art techniques in terms of accuracy, sensitivity, precision and f1 score. Table 4 shows the performance metrics of the proposed model, whereas Table 5 depicts the comparison of it with the state-of-the-art techniques (performance measures are adopted from the literature). The three-class classification accuracy of the proposed COVID DeepNet model is 99.67%. According to Shoeibi et al.'s review reports, the accuracies of state-of-the-art AI deep learning techniques in COVID-19 detection using lung X-rays range from 90 to 100 percent [6]. Consequently, the performance of our proposed model complies with the most recent state-of-the-art.

The disadvantage with all the other reported methods was the size of the COVID-19 lung X-ray database, which was considered for the experimentation. This is quite obvious from Table 5. Another disadvantage was the size of the input image fed to the deep learning model. As the input image size increased, the computational complexity and the time requisite for the training were also observed to be growing. Compared to all the other authors Sohaib Asif et al. considered X-ray images of reasonable sample size (COVID-19[864], Pneumonia[1345], and normal[1341]) [38]. However, the dataset they have considered is quite unbalanced, which is not desirable for an unbiased classification.

This research explored a balanced dataset to avoid network bias. For the experiment, a database with 2500 X-ray images for COVID-19, non-COVID Pneumonia, and normal was constructed with tremendous effort. The performance of the proposed COVID-DeepNet model is comparable or better (in terms of accuracy, sensitivity, precision, and f1 score) than the other related methods in the literature. This result demonstrates that the proposed COVID DeepNet model can accurately and precisely differentiate COVID-19, non-COVID Pneumonia, and normal X-ray images for symptomatic patients. The advantage of the proposed model is its architectural simplicity with fewer Deep layers. The internal architecture depicted in Table 2 demonstrates the proposed model's architectural simplicity. The computational burden and time for processing the Deep networks were remarkably reduced by resizing the X-ray images to an optimal size (64×64) without eliminating the relevant features and compromising the classification accuracy. This feature is a great boon while training the network, such as the proposed COVID-DeepNet model. The performance comparison demonstrates the efficacy of the reported approach for the three-class classification of lung X-

Table 5
Comparison of the proposed method with state-of-the-art techniques.

No	Author	Database	Method	Performance metrics			
		[COVID-19, Pneumonia, Normal]		Accuracy	Sensitivity	Precision	f1-score
1	Tulin Ozturk et al. [11]	[125, 500, 500]	DarkCovidNet	0.8702	0.8535	0.8996	0.8737
2	Khalid El Asnaoui et al. [20]	[231, 2780, 1583]	Densnet201	0.8809	0.8799	0.8852	0.8791
3	Khalid El Asnaoui et al. [20]	[231, 2780, 1583]	Inception-ResNet-V2	0.9218	0.9211	0.9238	0.9207
4	Wang L, Wong A [32]	[358, 5538, 8066]	COVID-Net	0.9330	0.9333	–	0.9000
5	Rubina Sarki et al. [33]	[296, 3875, 1341]	CNN	0.9375	1.0000	–	–
6	Laboni Sarker et al. [34]	[140, 140, 140]	Densenet-121	0.9400	0.9400	0.9400	0.9400
7	R. Murugan et al. [35]	[900, 900, 900]	E-DiCoNet	0.9407	0.9815	0.9815	0.9122
8	Antonios Makris et al. [36]	[112, 112, 112]	VGG16	0.9588	0.9560	0.9500	0.9560
9	Manu Siddhartha et al. [37]	[536, 619, 668]	COVIDLite	0.9643	0.9600	0.9700	0.9600
10	Ioannis D. Apostolopoulos et.al. [19]	[224, 700, 504]	VGG19	0.9678	0.9866	–	–
11	Sohaib Asif et al. [38]	[864, 1345, 1341]	Inception V3	0.9800	–	–	–
12	Rajeev Kumar Singh et al. [39]	[1519, 1519, 1519]	COVIDScreen	0.9867	–	–	0.9866
13	N. Narayan Das et al. [40]	[125, 500, 500]	Inception Model	0.9952	0.9912	–	0.9863
14	Mesut et al. [41]	[295, 98, 65]	MobileNetV2 SqueezeNet	0.9927	0.9833	0.9889	0.9857
15	Proposed Method	[2500, 2500, 2500]	COVID-DeepNet	0.9967	0.9965	0.9966	0.9966

ray images into COVID-19, non-COVID Pneumonia, and normal using a reasonable dataset size.

4.4. Limitations and future work

Data accessibility and fixing of AI deep learning architecture are two significant challenges that we faced in the automatic detection of COVID-19. The proposed model's limitations are due to the dataset's limitations. Due to the scarcity of high-quality COVID-19 public images, the current research considered only a modest data set size (2500 for each disease). The number of layers and nodes and the number of parameters in different layers can be optimized in the future. The selection of the learning rate, number of epochs, and regularisation intensity, the structuring and optimization of the network layers and nodes all require skill and expertise. More robust models can be developed in the future by combining data from multiple sources. Chest X-rays can also be used to examine the detection of mutated COVID-19 viral infection. We have only trained the model for three classes so far, but incorporating more, such as ARDS (acute respiratory distress syndrome), DERS (difficulties in emotion regulation), SARS bacterial and viral pneumonia, would make it even more robust. Our COVID DeepNet model only considered infection in the lungs for COVID-19 screening, which can only be used for symptomatic patients. Other influential symptoms can be validated using a suitable model and combined with the existing model to achieve a more precise result.

5. Conclusions

In this paper, a novel, highly efficient, and accurate COVID-DeepNet model is proposed to detect COVID-19 from the lung X-ray images of acutely symptomatic patients. The reported model is robust, and it executes a multi-class classification of X-ray images into COVID-19, non-COVID Pneumonia, and normal with a superior classification accuracy of 99.67%. The performance of the proposed model was evaluated in terms of accuracy, sensitivity, precision, and f1 score using a sample size of 7500 lung X-ray images, out of which only 80% were used in the training process. The proposed model exhibited impressive multi-class classification accuracy of X-ray images compared to state-of-the-art methods for the given sample size. The suggested system is equipped to assist radiologists in the rapid COVID-19 diagnosis and differentiate it from non-COVID Pneumonia. Hence, this research has substantial clinical significance as it improves the rapid identification and pre-screening of the existence of COVID-19 infection before the results of the RT-PCR test are made available. Furthermore, the financial burden incurred in the cost of diagnosis of the deadly disease can be reduced drastically.

Credit author statement

All the authors had equally contributed towards the work and writing of the manuscript.

Declaration of Competing Interest

The authors state that the work was carried out in the absence of any commercial and financial agreements that could be regarded as a potential conflict of interest.

References

[1] N. Jebril, World health organization declared a pandemic public health menace: a systematic review of the coronavirus disease 2019 "covid-19", Int. J. Psychosoc. Rehabil. 24 (2020) 9160–9166, https://doi.org/10.37200/IJPR/V24I9/PR290311.

[2] N. Kandel, S. Chungong, A. Omaar, J. Xing, Health security capacities in the context of covid-19 outbreak: an analysis of international health regulations annual report data from 182 countries, Lancet 395 (10229) (2020) 1047–1053, https://doi.org/10.1016/S0140-6736(20)30553-5.

[3] D. Shen, Y. Gao, A. Munoz-Barrutia, D.C. Debuc, G. Percannella, Guest editorial: special issue on imaging-based diagnosis of covid-19, IEEE Trans. Med. Imaging 39 (8) (2020) 2569–2571, https://doi.org/10.1109/TMI.2020.3008025.

[4] C. Sohrabi, Z. Alsafi, N. O'Neill, M. Khan, A. Kerwan, A. Al-Jabir, C. Iosifidis, R. Agha, World health organization declares global emergency: a review of the 2019 novel coronavirus (covid-19), Int. J. Surg. 76 (2020) 71–76, https://doi.org/10.1016/j.ijsu.2020.02.034.

[5] M. Otoom, N. Otoum, M.A. Alzubaidi, Y. Etoom, R. Banihani, An iot-based framework for early identification and monitoring of covid-19 cases, Biomed. Signal Process. Control 62 (2020) 102149, https://doi.org/10.1016/j.bspc.2020.102149.

[6] A. Shoeibi, M. Khodatars, R. Alizadehsani, N. Ghassemi, M. Jafari, P. Moridian, A. Khadem, D. Sadeghi, S. Hussain, A. Zare, et al., Automated Detection and Forecasting of Covid-19 Using Deep Learning Techniques: A Review, 2020 (arXiv preprint), arXiv:2007.10785.

[7] WHO, World Health Organization Coronavirus Disease (Covid-19) Dashboard, 2021. https://covid19.who.int/.

[8] H. Flick, B.-M. Arns, J. Bolitschek, B. Bucher, K. Cima, E. Gingrich, S. Handzhiev, M. Hochmair, F. Horak, M. Idzko, et al., Management of patients with sars-cov-2 infections and of patients with chronic lung diseases during the covid-19 pandemic (as of 9 may 2020), Wien. Klin. Wochenschr. 132 (13) (2020) 365–386, https://doi.org/10.1007/s00508-020-01691-0.

[9] H. Kang, L. Xia, F. Yan, Z. Wan, F. Shi, H. Yuan, H. Jiang, D. Wu, H. Sui, C. Zhang, D. Shen, Diagnosis of coronavirus disease 2019 (covid-19) with structured latent multi-view representation learning, IEEE Trans. Med. Imaging 39 (8) (2020) 2606–2614, https://doi.org/10.1109/TMI.2020.2992546.

[10] S. Muhammad, X. Long, M. Salman, Covid-19 pandemic and environmental pollution: a blessing in disguise? Sci. Total Environ. 728 (2020) 138820, https://doi.org/10.1016/j.scitotenv.2020.138820.

[11] T. Ozturk, M. Talo, E.A. Yildirim, U.B. Baloglu, O. Yildirim, U.R. Acharya, Automated detection of covid-19 cases using deep neural networks with x-ray images, Comput. Biol. Med. 121 (2020) 103792, https://doi.org/10.1016/j.compbiomed.2020.103792.

[12] A. Rothan, N. Hussin, Byrareddy, Siddappa, The epidemiology and pathogenesis of coronavirus disease (covid-19) outbreak, J. Autoimmun. 109 (2020) 102433, https://doi.org/10.1016/j.jaut.2020.102433.

[13] T. Singhal, A review of coronavirus disease-2019 (covid-19), Indian J. Pediatr. 87 (4) (2020) 281–286, https://doi.org/10.1007/s12098-020-03263-6.

[14] T. Ai, Z. Yang, H. Hou, C. Zhan, C. Chen, W. Lv, Q. Tao, Z. Sun, L. Xia, Correlation of chest ct and rt-pcr testing in coronavirus disease 2019 (covid-19) in China: a report of 1014 cases, Radiology 296 (2) (2020) 200642, https://doi.org/10.1148/radiol.2020200642.

[15] B. Robson, Computers and viral diseases. preliminary bioinformatics studies on the design of a synthetic vaccine and a preventative peptidomimetic antagonist against the sars-cov-2 (2019-ncov, covid-19) coronavirus, Comput. Biol. Med. 119 (2020) 103670, https://doi.org/10.1016/j.compbiomed.2020.103670.

[16] S.R. Nayak, D.R. Nayak, U. Sinha, V. Arora, R.B. Pachori, Application of deep learning techniques for detection of covid-19 cases using chest x-ray images: a comprehensive study, Biomed. Signal Process. Control 64 (2021) 102365, https://doi.org/10.1016/j.bspc.2020.102365.

[17] A. Panthakkan, S. Anzar, S.A. Mansoori, H.A. Ahmad, Accurate prediction of covid-19 (+) using ai deep vgg16 model, 2020 3rd International Conference on Signal Processing and Information Security (ICSPIS) (2020) 1–4, https://doi.org/10.1109/ICSPIS51252.2020.9340145.

[18] A. Bhandary, G.A. Prabhu, V. Rajinikanth, K.P. Thanaraj, S.C. Satapathy, D. E. Robbins, C. Shasky, Y.-D. Zhang, J.M.R. Tavares, N.S.M. Raja, Deep-learning framework to detect lung abnormality- a study with chest x-ray and lung ct scan images, Pattern Recognit. Lett. 129 (2020) 271–278, https://doi.org/10.1016/j.patrec.2019.11.013.

[19] I.D. Apostolopoulos, T.A. Mpesiana, Covid-19: automatic detection from x-ray images utilizing transfer learning with convolutional neural networks, Phys. Eng. Sci. Med. 43 (2020) 635–640, https://doi.org/10.1007/s13246-020-00865-4.

[20] K.E. Asnaoui, Y. Chawki, Using x-ray images and deep learning for automated detection of coronavirus disease, J. Biomol. Struct. Dyn. (2020) 1–12, https://doi.org/10.1080/07391102.2020.1767212.

[21] M. Alazab, A. Awajan, A. Mesleh, A. Abraham, V. Jatana, S. Alhyari, Covid-19 prediction and detection using deep learning, Int. J. Comput. Inf. Syst. Ind. Manag. Appl. 12 (2020) 168–181.

[22] K. Simonyan, A. Zisserman, Very Deep Convolutional Networks for Large-Scale Image Recognition, 2014 (arXiv preprint), arXiv:1409.1556v6.

[23] H. Farhat, G.E. Sakr, R. Kilany, Deep learning applications in pulmonary medical imaging: recent updates and insights on covid-19, Mach. Vis. Appl. 31 (6) (2020) 53, https://doi.org/10.1007/s00138-020-01101-5.

[24] T. Nepusz, A. Petróczi, L. Négyessy, F. Bazsó, Guest editorial deep learning in medical imaging: overview and future promise of an exciting new technique, IEEE Trans. Med. Imaging 35 (2016) 1153–1159, https://doi.org/10.1109/TMI.2016.2553401.

[25] A.S. Glassner, Deep Learning: From Basics to Practice, vol. 1, The Imaginary Institute, Seattle, WA, 2018.

[26] L. Brunese, F. Mercaldo, A. Reginelli, A. Santone, Explainable deep learning for pulmonary disease and coronavirus covid-19 detection from x-rays, Comput. Methods Programs Biomed. 196 (2020) 105608, https://doi.org/10.1016/j.cmpb.2020.105608.

[27] J.F.-W. Chan, S. Yuan, K.-H. Kok, K.K.-W. To, H. Chu, J. Yang, F. Xing, J. Liu, C.C.-Y. Yip, R.W.-S. Poon, et al., A familial cluster of pneumonia associated with the 2019 novel coronavirus indicating person-to-person transmission: a study of a

family cluster, Lancet 395 (2020) 514–523, https://doi.org/10.1016/S0140-6736(20)30154-9.
[28] M.-Y. Ng, E.Y. Lee, J. Yang, F. Yang, X. Li, H. Wang, M.M.-s. Lui, C.S.-Y. Lo, B. Leung, P.-L. Khong, et al., Imaging profile of the covid-19 infection: radiologic findings and literature review, Radiol. Cardiothorac. Imaging 2 (1) (2020) e200034, https://doi.org/10.1148/ryct.2020200034.
[29] H. Shi, X. Han, N. Jiang, Y. Cao, O. Alwalid, J. Gu, Y. Fan, C. Zheng, Radiological findings from 81 patients with covid-19 pneumonia in Wuhan, China: a descriptive study, Lancet Infect. Dis. 20 (4) (2020), https://doi.org/10.1016/S1473-3099(20)30086-4.
[30] A. Bernheim, X. Mei, M. Huang, Y. Yang, Z.A. Fayad, N. Zhang, K. Diao, B. Lin, X. Zhu, K. Li, et al., Chest ct findings in coronavirus disease-19 (covid-19): relationship to duration of infection, Radiology 295 (3) (2020) 200463, https://doi.org/10.1148/radiol.2020200463.
[31] S. Vaid, R. Kalantar, M. Bhandari, Deep learning covid-19 detection bias: accuracy through artificial intelligence, Int. Orthop. 44 (2020) 1539–1542, https://doi.org/10.1007/s00264-020-04609-7.
[32] L. Wang, A. Wong, Covid-net: a tailored deep convolutional neural network design for detection of covid-19 cases from chest x-ray images, Sci. Rep. 10 (2020), 19549, https://doi.org/10.1038/s41598-020-76550-z.
[33] R. Sarki, K. Ahmed, H. Wang, Y. Zhang, K. Wang, Automated Detection of Covid-19 Through Convolutional Neural Network Using Chest X-ray Images, 2021 medRxiv.
[34] L. Sarker, M.M. Islam, T. Hannan, Z. Ahmed, Covid-Densenet: A Deep Learning Architecture to Detect Covid-19 From Chest Radiology Images, 2020, https://doi.org/10.20944/preprints202005.0151.v1.
[35] R. Murugan, T. Goel, E-diconet: extreme learning machine based classifier for diagnosis of covid-19 using deep convolutional network, J. Ambient Intell. Humaniz. Comput. (2021) 1–12, https://doi.org/10.1007/s12652-020-02688-3.
[36] A. Makris, I. Kontopoulos, K. Tserpes, Covid-19 detection from chest X-ray images using deep learning and convolutional neural networks. 11th Hellenic Conference on Artificial Intelligence, Association for Computing Machinery, New York, NY, USA, 2020, pp. 60–66, https://doi.org/10.1145/3411408.3411416.
[37] M. Siddhartha, A. Santra, Covidlite: A Depth-Wise Separable Deep Neural Network With White Balance and Clahe for Detection of Covid-19, 2020 (arXiv preprint), arXiv:2006.13873.
[38] S. Asif, Y. Wenhui, H. Jin, Y. Tao, S. Jinhai, Classification of Covid-19 From Chest X-ray Images Using Deep Convolutional Neural Networks, 2020, https://doi.org/10.1007/s10489-020-01829-7 medRxiv.
[39] R.K. Singh, R. Pandey, R.N. Babu, Covidscreen: explainable deep learning framework for differential diagnosis of covid-19 using chest X-rays, Neural Comput. Appl. (2021) 1–22.
[40] N. Narayan Das, N. Kumar, M. Kaur, V. Kumar, D. Singh, Automated Deep Transfer Learning-Based Approach for Detection of Covid-19 Infection in Chest X-rays, IRBM, 2020, https://doi.org/10.1016/j.irbm.2020.07.001.
[41] M. Toğaçar, B. Ergen, Z. Cömert, Covid-19 detection using deep learning models to exploit social mimic optimization and structured chest X-ray images using fuzzy color and stacking approaches, Comput. Biol. Med. 121 (2020) 103805, https://doi.org/10.1016/j.compbiomed.2020.103805.
[42] Y. LeCun, L. Bottou, Y. Bengio, P. Haffner, Gradient-based learning applied to document recognition, Proc. IEEE 86 (11) (1998) 2278–2324, https://doi.org/10.1109/5.726791.
[43] J. Gu, Z. Wang, J. Kuen, L. Ma, A. Shahroudy, B. Shuai, T. Liu, X. Wang, G. Wang, J. Cai, et al., Recent advances in convolutional neural networks, Pattern Recognit. 77 (2018) 354–377, https://doi.org/10.1016/j.patcog.2017.10.013.
[44] D. Das, K. Santosh, U. Pal, Truncated inception net: covid-19 outbreak screening using chest X-rays, Phys. Eng. Sci. Med. (2020) 915–925, https://doi.org/10.1007/s13246-020-00888-x.
[45] D. Singh, V. Kumar, M. Kaur, Classification of covid-19 patients from chest ct images using multi-objective differential evolution-based convolutional neural networks, Eur. J. Clin. Microbiol. Infect. Dis. 39 (7) (2020) 1–11, https://doi.org/10.1007/s10096-020-03901-z.
[46] D.P. Kingma, J. Ba, Adam: A Method for Stochastic Optimization, 2017 (arXiv preprint), arXiv:1412.6980v9.
[47] J.P. Cohen, P. Morrison, L. Dao, K. Roth, T.Q. Duong, M. Ghassemi, Covid-19 Image Data Collection: Prospective Predictions are the Future, 2020 06 (arXiv preprint), arXiv:2006.11988v3.
[48] X. Wang, Y. Peng, L. Lu, Z. Lu, M. Bagheri, R.M. Summers, Chestx-ray8: Hospital-Scale Chest X-ray Database and Benchmarks on Weakly-Supervised Classification and Localization of Common Thorax Diseases, 2017, pp. 2097–2106.
[49] A. Narin, C. Kaya, Z. Pamuk, Automatic Detection of Coronavirus Disease (Covid-19) Using X-ray Images and Deep Convolutional Neural Networks, 2020 10 (arXiv preprint), arXiv:arXiv:2003.10849v3.
[50] J. Civit-Masot, F. Luna-Perejón, M. Domínguez Morales, A. Civit, Deep learning system for covid-19 diagnosis aid using x-ray pulmonary images, Appl. Sci. 10 (13) (2020) 6125–6134, https://doi.org/10.3390/app10134640.

Dr. Alavikunhu Panthakkan is a dynamic research scientist in Electronics Engineering and he is working as an Assistant Professor at the College of Engineering and IT, University of Dubai. His research interests are in the areas of engineering education, copyright protection, authentication, medical image processing, video signal processing, and Artificial Neural Network (ANN). He received a Ph.D. in Electronics Engineering. He is a member of IEEE, a member of the Institution of Engineers (India) (MIE), member of International Association of Engineers (IAENG), member of International Association of Computer and Information Technology (IACSIT), and member of Institute of Research Engineers and Doctors (IRED).

Dr. S. M. Anzar is the faculty in the Electronics and Communication Engineering Department at TKM College of Engineering Kollam, India. His research interests include (Medical) Signal and Image processing, Pattern Recognition, Bio-metrics, and Artificial Intelligence. He received a Ph.D. degree from the National Institute of Technology Calicut, India in 2014. He obtained his Masters in Engineering (M.E.) Degree in Applied Electronics from Anna University, Chennai in 2008 and Bachelor of Technology (B.Tech.) Degree in Electronics and Instrumentation Engineering from CUSAT, Cochin in 2003. He is a member of the IEEE, IEEE Signal Processing Society, and Indian Society for Technical Education (ISTE).

Eng. Saeed Al Mansoori is the head of the Applications Development and Analysis Section (ADAS) at Mohammed Bin Rashid Space Center. He has received a B.Sc. degree in communication engineering from Khalifa University of Science, Technology, and Research (KUSTAR), Sharjah, UAE in 2010 and the M.Sc. degree in Electrical Engineering from American University of Sharjah (AUS) in 2016. Saeed's research interests are in the area of image processing (super-resolution, watermarking, object detection, and image classification). He is a member of the international society of optics and photonics and one of the program committees in High-Performance Computing in Remote Sensing since 2012.

Prof. Hussain Al Ahmad got his Ph.D. from the University of Leeds, UK in 1984 and he is the founding Dean of Engineering and IT at the University of Dubai, UAE. He has 33 years of higher education experience working at academic institutions in different countries. His research interests are in the areas of engineering education, signal and image processing, multimedia, remote sensing, and propagation. He is a Senior Member of the IEEE and a Fellow of the Institution of Engineering and Technology (FIET), Chartered Engineer (C.Eng), Member of BCS The Chartered Institute for IT (MBCS), Chartered IT Professional (CITP), Fellow of the British Royal Photographic Society (FRPS), Accredited Senior Imaging Scientist (ASIS). He is the Chairman of the IEEE UAE Education Chapter and Vice Chairman of the Middle East Section of BCS. He was a founder member and Ex. Chairman of the IEEE UAE Computer Chapter and Ex-Vice Chairman of the IEEE UAE Signal Processing and Communication Chapter. He was also the founder member and Ex-Secretary of the IEEE Kuwait section.